

Chapter 3

Investigation of Three-Body Interactions on the Phase Behaviour of Noble Gases

In the following sections we report the results obtained studying the role of three-body interatomic potentials on noble gas coexisting phases. Section 3.1 gives details of the Gibbs ensemble simulations for vapour-liquid coexisting phases of argon, krypton and xenon as pure fluids and of an argon-krypton mixture. In section 3.2 we report the analytic expression of an effective potential which we found to reproduce the main feature of the two-body + three-body potentials. The significance of this relationship is that three-body interactions can be estimated with sufficient accuracy from two-body interactions without incurring the computational penalty of three-body calculations. The relationship has the potential of improving both the accuracy and predictive value of pair interaction molecular simulations.

3.1 Vapour-liquid coexisting phases of noble gases

The aim of this work is to investigate the role of the dipole-dipole-dipole term and other multipole three-body dispersion terms on the vapour-liquid phases observed for argon, krypton and xenon. As discussed in Chapter 2, we have used the potentials

proposed by Barker et al. [Bar71a, Bar74, see Eqs. (2.11), (2.12) and (2.13)] for the two-body interactions. The three-body interactions were obtained from considering the dipole-dipole-dipole (third-order DDD or Axilrod-Teller term, Eq. (2.17)), the dipole-dipole-quadrupole (third-order DDQ , Eq. (2.18)) the dipole-quadrupole-quadrupole (third-order DQQ , Eq. (2.19)), quadrupole-quadrupole-quadrupole (third-order QQQ , Eq. (2.20)) and the dipole-dipole-dipole (forth-order DDD , Eq. (2.21)).

3.1.1 Simulation details

Pure fluids

The NVT Gibbs ensemble technique (for details see Chapter 2) was implemented for a system of 500 atoms. The simulations were performed in cycles consisting typically of 500 attempted displacements, an attempted volume change and 500 interchange attempts. Typically, 1000-1500 cycles were used for equilibration and a further 1500-2000 cycles were used to accumulate ensemble averages. The normal convention was adopted for the reduced density ($\mathbf{r}^* = \mathbf{r}\mathbf{s}^3$), temperature ($T^* = kT/\epsilon$), energy ($E^* = E/\epsilon$), pressure ($P^* = P\mathbf{s}^3/\epsilon$) and chemical potential ($\mathbf{m}^* = \mathbf{m}\epsilon$).

Periodic boundary conditions were applied. The two-body potentials were truncated at half the box length and appropriate long range correction terms (see Appendix 1) were evaluated to recover the contribution to pressure, energy and chemical potential of the full intermolecular potential. Some care needs to be taken with the three-body potentials because the application of a periodic boundary can potentially destroy the position-invariance of three particles (see Appendix 2). We examined the behaviour of the three-body terms for many thousands of different configurations and intermolecular separations. All the three-body terms asymptote rapidly to zero with increasing

intermolecular separation. For a system size of 500 or more atoms, we found truncating the three-body potentials at intermolecular separations greater than a quarter of the length of the simulation box to be an excellent approximation to the full potential that also avoided the problem of three-body invariance to periodic boundary conditions.

The chemical potential was determined from the equation proposed by Smit et al. [Smi89a, see Chapter 2]. The uncertainties in the ensemble averages for density, temperature, energy and pressure were calculated by dividing the post-equilibrium results into ten sections. The estimated errors represent the standard deviations of the section averages. An error estimate for the chemical potential cannot be estimated in this way because it is the average of the entire post-equilibrium simulation.

Binary mixture

The *NPT* Gibbs ensemble technique was used for an argon-krypton mixture. The details of the simulations are similar to those discussed above for the pure fluids. In this work we analyzed the pressure-composition behaviour of the mixture and compared it with experimental data. The pressure-density behaviour was also studied.

The intermolecular potentials mentioned previously were developed originally for pure fluids, but they can be applied directly to binary mixtures by assuming suitable combining rules for the intermolecular parameters. In general if we denote the energy-like parameters \mathbf{n} and \mathbf{e} (see Chapter 2) by the symbol W , the cross potential parameters of interacting pairs and triplets can be calculated from:

$$\left. \begin{aligned} W_{ijk} &= \sqrt[3]{W_{iii}W_{jjj}W_{kkk}} \\ W_{ij} &= \sqrt[2]{W_{ii}W_{jj}} \end{aligned} \right\} \quad (3.1)$$

In general if we denote all the remaining parameters such as \mathbf{s} , A , C_6 etc (see Chapter 2) by the symbol Y , the cross potential parameters of interacting pairs can be calculated from:

$$Y_{ij} = \frac{Y_{ii} + Y_{jj}}{2} \quad (3.2)$$

In the argon-krypton mixture simulations the potential parameters of argon \mathbf{e} and \mathbf{s} were used to obtain reduced quantities in the standard way. It is important to stress that these commonly used combining rules do not have physical rationale.

The three-body simulations commonly require 20 and 12 CPU hrs on the Fujitsu VPP300 and NEC SX-4/32 supercomputers, respectively.

3.1.2 Results and discussion

Pure fluids

The results of Gibbs ensemble simulations for the vapour-liquid properties of argon, krypton and xenon are reported in Tables 3.1-3.6. A comparison of simulation results with experiment is given in Figures 3.1, 3.3 and 3.4. The relative contribution to energy of the various three-body interactions for the liquid phase of argon is illustrated in Figure 3.2. The total pressure versus the temperature is reported in Figure 3.5.

Table 3.1 Vapour-liquid coexistence properties of argon from molecular simulation using the two-body BFW potential [Bar71a].

T^*	r_L^*	P_L^*	E_L^*	m_L^*	r_V^*	P_V^*	E_V^*	m_V^*
0.700	0.806(4)	-0.018(38)	-5.18(3)	-3.67	0.006(1)	0.004(1)	-0.06(2)	-3.70
0.750	0.781(3)	0.007(21)	-4.98(2)	-3.67	0.008(1)	0.006(1)	-0.08(3)	-3.68
0.825	0.741(4)	0.020(14)	-4.66(3)	-3.43	0.021(2)	0.015(2)	-0.19(3)	-3.39
0.850	0.727(5)	0.022(19)	-4.56(3)	-3.49	0.023(2)	0.017(3)	-0.21(3)	-3.42
0.875	0.711(5)	0.017(16)	-4.44(4)	-3.47	0.030(2)	0.022(3)	-0.26(3)	-3.36
0.900	0.696(5)	0.022(19)	-4.33(4)	-3.39	0.033(3)	0.025(3)	-0.29(3)	-3.38
0.925	0.678(3)	0.036(10)	-4.20(2)	-3.40	0.041(2)	0.031(3)	-0.35(3)	-3.32
0.950	0.661(10)	0.037(22)	-4.08(6)	-3.35	0.049(5)	0.037(7)	-0.41(4)	-3.30
0.975	0.644(6)	0.049(16)	-3.97(4)	-3.34	0.057(5)	0.042(6)	-0.47(4)	-3.28
1.000	0.622(7)	0.056(13)	-3.81(4)	-3.24	0.073(7)	0.051(12)	-0.59(6)	-3.23
1.025	0.597(8)	0.062(17)	-3.66(5)	-3.25	0.082(6)	0.058(11)	-0.64(6)	-3.23
1.050	0.574(9)	0.071(21)	-3.50(5)	-3.22	0.104(7)	0.069(13)	-0.82(6)	-3.18
1.075	0.540(12)	0.080(27)	-3.31(7)	-3.20	0.112(10)	0.075(19)	-0.86(8)	-3.20

Table 3.2 Vapour-liquid coexistence properties of krypton from molecular simulation using the two-body Barker et al. potential [Bar74].

T^*	r_L^*	P_L^*	E_L^*	m_L^*	r_V^*	P_V^*	E_V^*	m_V^*
0.700	0.800(4)	-0.002(33)	-5.05(3)	-3.58	0.007(2)	0.005(1)	-0.07(3)	-3.55
0.750	0.774(3)	0.001(21)	-4.84(3)	-3.55	0.010(1)	0.007(1)	-0.09(2)	-3.53
0.825	0.735(5)	0.020(19)	-4.53(4)	-3.39	0.024(2)	0.017(2)	-0.21(2)	-3.31
0.850	0.718(4)	0.013(12)	-4.41(3)	-3.35	0.026(2)	0.019(2)	-0.22(3)	-3.34
0.875	0.700(5)	0.020(15)	-4.28(4)	-3.33	0.031(4)	0.023(4)	-0.27(4)	-3.32
0.900	0.687(5)	0.034(12)	-4.18(3)	-3.28	0.041(4)	0.030(4)	-0.36(4)	-3.24
0.925	0.666(7)	0.036(16)	-4.04(4)	-3.26	0.048(7)	0.034(10)	-0.41(7)	-3.23
0.950	0.647(3)	0.044(13)	-3.91(2)	-3.23	0.059(3)	0.041(5)	-0.48(3)	-3.18
0.975	0.624(9)	0.048(18)	-3.76(6)	-3.19	0.067(5)	0.047(7)	-0.54(4)	-3.18
1.000	0.609(6)	0.065(14)	-3.66(3)	-3.16	0.087(4)	0.059(7)	-0.68(5)	-3.12
1.025	0.573(17)	0.073(26)	-3.44(9)	-3.16	0.098(12)	0.065(20)	-0.75(8)	-3.13
1.050	0.548(18)	0.084(31)	-3.28(9)	-3.12	0.131(18)	0.080(33)	-0.98(14)	-3.09
1.065	0.530(23)	0.094(46)	-3.18(12)	-3.11	0.141(16)	0.082(33)	-1.05(11)	-3.08

Table 3.3 Vapour-liquid coexistence properties of xenon from molecular simulation using the two-body Barker et al. potential [Bar74].

T^*	r_L^*	P_L^*	E_L^*	m_L^*	r_V^*	P_V^*	E_V^*	m_V^*
0.700	0.801(5)	-0.010(36)	-5.07(3)	-3.72	0.006(1)	0.004(1)	-0.06(2)	-3.63
0.750	0.777(4)	-0.005(21)	-4.88(3)	-3.43	0.011(2)	0.008(1)	-0.10(2)	-3.49
0.825	0.733(4)	0.005(15)	-4.54(2)	-3.32	0.022(3)	0.016(3)	-0.20(4)	-3.35
0.850	0.715(6)	0.021(20)	-4.41(4)	-3.42	0.027(3)	0.020(3)	-0.24(3)	-3.32
0.875	0.701(3)	0.027(20)	-4.31(2)	-3.37	0.032(3)	0.023(4)	-0.28(3)	-3.30
0.900	0.682(4)	0.026(19)	-4.17(3)	-3.34	0.037(3)	0.027(4)	-0.32(3)	-3.29
0.925	0.664(8)	0.031(16)	-4.05(5)	-3.28	0.047(6)	0.034(7)	-0.39(4)	-3.24
0.950	0.644(9)	0.038(22)	-3.91(6)	-3.25	0.055(3)	0.040(4)	-0.46(3)	-3.22
0.975	0.623(9)	0.045(21)	-3.77(6)	-3.20	0.068(6)	0.048(10)	-0.55(7)	-3.18
1.000	0.605(9)	0.063(23)	-3.65(6)	-3.18	0.082(6)	0.056(10)	-0.65(4)	-3.15
1.025	0.583(11)	0.072(19)	-3.51(7)	-3.15	0.099(9)	0.066(15)	-0.77(6)	-3.12
1.050	0.549(14)	0.083(27)	-3.30(8)	-3.15	0.123(10)	0.077(19)	-0.94(8)	-3.10
1.075	0.501(88)	0.103(183)	-3.02(48)	-3.10	0.160(17)	0.088(34)	-1.18(12)	-3.07

Table 3.4 Vapour-liquid coexistence properties of argon from molecular simulation using the two-body BFW potential [Bar71a] + three-body ($DDD + DDQ + DQQ + DDD4$) intermolecular potentials.

	T^*									
	0.750	0.825	0.850	0.875	0.900	0.925	0.950	0.975	1.00	
r^*_L	0.742(5)	0.685(8)	0.671(10)	0.658(10)	0.639(11)	0.613(11)	0.600(10)	0.564(11)	0.513(30)	
P^*_{Ltot}	0.044(89)	0.017(38)	0.020(50)	0.028(41)	0.033(52)	0.035(41)	0.049(36)	0.045(39)	0.052(100)	
P^*_{L2body}	-0.914(77)	-0.854(21)	-0.825(30)	-0.809(21)	-0.788(30)	-0.743(20)	-0.718(17)	-0.673(19)	-0.591(51)	
P^*_{LDD}	0.375(8)	0.271(9)	0.250(10)	0.235(8)	0.218(9)	0.190(9)	0.175(7)	0.149(7)	0.117(15)	
P^*_{LDDQ}	0.125(3)	0.090(3)	0.083(3)	0.078(3)	0.072(3)	0.062(3)	0.057(2)	0.049(3)	0.038(5)	
P^*_{LDDQ}	0.0254(7)	0.0186(7)	0.0170(7)	0.0159(6)	0.0147(6)	0.0127(7)	0.0117(6)	0.0099(6)	0.0076(11)	
P^*_{LQQQ}	0.0023(1)	0.0017(1)	0.0015(1)	0.0014(1)	0.0013(1)	0.0011(1)	0.0010(1)	0.0009(1)	0.0007(1)	
P^*_{LDD4}	-0.124(3)	-0.074(2)	-0.068(2)	-0.063(2)	-0.058(1)	-0.052(2)	-0.046(1)	-0.040(1)	-0.033(3)	
$E^*_{Ltot conf}$	-4.53(3)	-4.13(6)	-4.01(7)	-3.97(5)	-3.89(7)	-3.68(6)	-3.57(6)	-3.39(6)	-3.09(16)	
E^*_{L2body}	-4.73(3)	-4.33(6)	-4.16(6)	-4.06(7)	-3.99(6)	-3.83(7)	-3.71(6)	-3.49(6)	-3.19(16)	
E^*_{LDD}	0.169(3)	0.132(3)	0.125(3)	0.119(3)	0.113(3)	0.103(3)	0.097(2)	0.088(3)	0.076(6)	
E^*_{LDDQ}	0.046(1)	0.036(1)	0.034(1)	0.032(1)	0.031(1)	0.028(1)	0.026(1)	0.023(1)	0.020(2)	
E^*_{LDDQ}	0.0079(2)	0.0063(2)	0.0059(2)	0.0056(1)	0.0053(1)	0.0048(2)	0.0045(1)	0.0040(2)	0.0034(3)	
E^*_{LQQQ}	0.00061(2)	0.00049(1)	0.00046(1)	0.00043(1)	0.00041(1)	0.00037(1)	0.00035(1)	0.00031(1)	0.00026(2)	
E^*_{LDD4}	-0.0419(10)	-0.0268(4)	-0.0256(4)	-0.0240(5)	-0.0227(4)	-0.0212(5)	-0.0192(4)	-0.0178(5)	-0.0161(7)	
m^*_L	-3.47	-3.48	-3.53	-3.40	-3.35	-3.36	-3.29	-3.26	-3.28	
r^*_V	0.0095(17)	0.0174(15)	0.0218(18)	0.0295(37)	0.0350(48)	0.0401(38)	0.0536(56)	0.0605(52)	0.0655(32)	
P^*_{Vtot}	0.0067(16)	0.0128(17)	0.0162(21)	0.0216(46)	0.0259(64)	0.0301(51)	0.0388(83)	0.0440(83)	0.0490(56)	
P^*_{V2body}	-0.0005(4)	-0.0016(4)	-0.0024(5)	-0.0043(13)	-0.0057(20)	-0.0071(15)	-0.0126(28)	-0.0155(31)	-0.0172(23)	
P^*_{VDD}	0.0005(22)	0.0212(156)	0.0432(198)	0.0846(533)	0.1350(726)	0.1911(609)	0.442(116)	0.567(145)	0.700(138)	
P^*_{VDDQ}	0.001(4)	0.070(65)	0.128(66)	0.249(172)	0.406(217)	0.572(188)	1.313(341)	1.67(418)	2.067(428)	
P^*_{VDQ}	0.001(6)	0.148(167)	0.239(142)	0.468(364)	0.775(418)	1.092(374)	2.486(636)	3.135(773)	3.896(864)	
P^*_{VQQQ}	0.001(4)	0.135(170)	0.198(132)	0.390(336)	0.659(362)	0.931(327)	2.106(532)	2.648(646)	3.307(779)	
P^*_{VDD4}	-0.0016(25)	-0.048(28)	-0.111(55)	-0.234(135)	-0.385(220)	-0.530(168)	-1.249(330)	-1.628(408)	-2.015(371)	
$E^*_{Vtot conf}$	-0.07(2)	-0.15(3)	-0.20(3)	-0.26(5)	-0.30(5)	-0.34(3)	-0.45(4)	-0.49(5)	-0.52(3)	
E^*_{V2body}	-0.07(2)	-0.15(3)	-0.20(3)	-0.26(5)	-0.30(5)	-0.34(3)	-0.46(4)	-0.49(5)	-0.52(3)	
E^*_{VDD}	0.02(7)	0.39(28)	0.64(28)	0.87(45)	1.21(49)	1.55(37)	2.65(46)	2.98(55)	3.47(60)	
E^*_{VDDQ}	0.003(10)	0.11(9)	0.16(8)	0.21(12)	0.30(12)	0.38(9)	0.65(11)	0.72(13)	0.84(16)	
E^*_{VDQ}	0.002(12)	0.19(20)	0.25(15)	0.33(23)	0.48(21)	0.62(16)	1.04(17)	1.14(20)	1.34(27)	
E^*_{VQQQ}	0.001(7)	0.15(18)	0.18(12)	0.24(18)	0.35(16)	0.46(13)	0.76(13)	0.84(15)	0.98(22)	
E^*_{VDD4}	-0.004(6)	-0.066(36)	-0.124(59)	-0.182(83)	-0.259(111)	-0.322(75)	-0.563(102)	-0.642(115)	-0.750(119)	
m^*_V	-3.57	-3.51	-3.46	-3.36	-3.34	-3.34	-3.25	-3.25	-3.26	

Table 3.5 Vapour-liquid coexistence properties of krypton from molecular simulation using the two-body Barker et al. [Bar74] + three-body ($DDD + DDQ + DQQ + DDD4$) intermolecular potentials.

	T^*									
	0.750	0.825	0.850	0.875	0.900	0.925	0.950	0.975		
r_V^*	0.712(6)	0.671(9)	0.642(9)	0.631(8)	0.616(7)	0.585(14)	0.528(23)	0.509(23)		
$P_{L, tot}^*$	0.051(75)	0.026(45)	0.028(35)	0.036(39)	0.040(26)	0.048(48)	0.045(77)	0.066(71)		
$P_{L, 2body}^*$	-0.899(46)	-0.848(23)	-0.807(15)	-0.784(21)	-0.758(12)	-0.703(20)	-0.616(40)	-0.573(34)		
$P_{L, DDD}^*$	0.390(25)	0.306(12)	0.273(9)	0.255(11)	0.233(7)	0.202(13)	0.157(13)	0.138(12)		
$P_{L, DDQ}^*$	0.127(9)	0.098(4)	0.088(3)	0.082(4)	0.074(2)	0.064(4)	0.049(4)	0.043(4)		
$P_{L, DQQ}^*$	0.0253(18)	0.0194(9)	0.0172(7)	0.0160(8)	0.0146(5)	0.0125(9)	0.0095(9)	0.0084(8)		
$P_{L, DDD4}^*$	0.0022(2)	0.0017(1)	0.0015(1)	0.0014(1)	0.00125(5)	0.0011(1)	0.0008(1)	0.0007(1)		
$E_{L, tot}^{* conf}$	-0.135(11)	-0.105(3)	-0.096(2)	-0.087(4)	-0.079(2)	-0.071(3)	-0.056(3)	-0.049(4)		
$E_{L, 2body}^*$	-4.28(3)	-3.98(6)	-3.83(5)	-3.72(5)	-3.59(4)	-3.43(8)	-3.13(10)	-3.00(11)		
$E_{L, DDD}^*$	-4.49(4)	-4.08(7)	-3.97(5)	-3.88(6)	-3.75(4)	-3.55(8)	-3.23(10)	-3.10(11)		
$E_{L, DDQ}^*$	0.183(11)	0.152(4)	0.141(3)	0.134(4)	0.126(2)	0.115(5)	0.098(4)	0.090(5)		
$E_{L, DQQ}^*$	0.049(3)	0.040(1)	0.037(1)	0.035(1)	0.033(1)	0.030(1)	0.025(1)	0.023(1)		
$E_{L, DDD4}^*$	0.0082(6)	0.0067(2)	0.0062(2)	0.0058(2)	0.0055(1)	0.0049(2)	0.0041(2)	0.0038(2)		
$E_{L, QQQ}^*$	0.00061(4)	0.00050(2)	0.00046(1)	0.00043(2)	0.00041(1)	0.00036(2)	0.00030(2)	0.00028(2)		
$E_{L, DDD4}^*$	-0.047(4)	-0.039(1)	-0.0372(5)	-0.035(1)	-0.032(1)	-0.030(1)	-0.027(1)	-0.024(1)		
m_L^*	-3.62	-3.37	-3.38	-3.24	-3.15	-3.24	-3.20	-3.17		
r_V^*	0.0105(12)	0.0203(15)	0.0246(20)	0.0348(37)	0.0429(17)	0.0477(31)	0.0578(33)	0.0737(61)		
$P_{V, tot}^*$	0.0074(12)	0.0148(18)	0.0183(25)	0.0253(50)	0.0316(25)	0.0350(45)	0.0409(46)	0.0507(104)		
$P_{V, 2body}^*$	-0.00005(3)	-0.0020(6)	-0.0027(8)	-0.0054(17)	-0.0073(9)	-0.0095(16)	-0.0146(14)	-0.0224(42)		
$P_{V, DDD}^*$	0.006(6)	0.0374(148)	0.0653(232)	0.171(77)	0.269(44)	0.338(67)	0.652(117)	1.20(29)		
$P_{V, DDQ}^*$	0.018(24)	0.111(42)	0.185(75)	0.497(228)	0.795(142)	0.971(183)	1.86(36)	3.44(85)		
$P_{V, DQQ}^*$	0.029(53)	0.205(81)	0.327(153)	0.908(423)	1.47(29)	1.74(32)	3.33(69)	6.22(1.58)		
$P_{V, DDD4}^*$	0.024(50)	0.168(71)	0.257(131)	0.738(345)	1.21(26)	1.40(25)	2.67(58)	5.05(1.31)		
$P_{V, DDD4}^*$	-0.036(24)	-0.127(34)	-0.225(58)	-0.601(255)	-0.978(156)	-1.27(26)	-2.38(40)	-4.40(1.08)		
$E_{V, tot}^{* conf}$	-0.09(2)	-0.18(3)	-0.21(2)	-0.29(4)	-0.36(2)	-0.38(3)	-0.47(3)	-0.58(6)		
$E_{V, 2body}^*$	-0.09(2)	-0.18(3)	-0.21(2)	-0.30(4)	-0.36(2)	-0.39(3)	-0.47(3)	-0.58(6)		
$E_{V, DDD}^*$	0.18(17)	0.59(22)	0.86(24)	1.56(55)	2.08(30)	2.31(33)	3.64(46)	5.27(90)		
$E_{V, DDQ}^*$	0.04(5)	0.14(5)	0.20(6)	0.37(14)	0.50(8)	0.54(7)	0.85(12)	1.24(22)		
$E_{V, DQQ}^*$	0.05(10)	0.23(9)	0.30(11)	0.58(23)	0.79(14)	0.82(11)	1.28(20)	1.89(35)		
$E_{V, DDD4}^*$	0.04(8)	0.16(7)	0.20(8)	0.41(16)	0.56(11)	0.57(8)	0.89(15)	1.33(26)		
$E_{V, DDD4}^*$	-0.082(50)	-0.149(38)	-0.222(48)	-0.411(138)	-0.567(77)	-0.649(94)	-0.996(113)	-1.45(25)		
m_V^*	-3.52	-3.40	-3.37	-3.25	-3.20	-3.21	-3.19	-3.13		

Table 3.6 Vapour-liquid coexistence properties of xenon from molecular simulation using the two-body Barker et al. [Bar74] + three-body ($BDD + DDQ + DQQ + DDD4$) intermolecular potentials.

	T^*									
	0.750	0.825	0.850	0.875	0.900	0.925	0.950	0.975		
r^*_L	0.706(6)	0.671(9)	0.634(12)	0.617(15)	0.599(11)	0.578(13)	0.517(23)	0.511(26)		
$P^*_{L, int}$	0.009(38)	0.024(53)	0.010(46)	0.030(64)	0.031(44)	0.059(61)	0.039(79)	0.060(89)		
$P^*_{V, 2body}$	-0.947(26)	-0.875(29)	-0.828(20)	-0.779(31)	-0.751(21)	-0.696(34)	-0.611(39)	-0.596(42)		
$P^*_{L, DDD}$	0.444(9)	0.364(15)	0.314(14)	0.288(18)	0.260(13)	0.235(14)	0.178(16)	0.169(20)		
$P^*_{L, DDQ}$	0.140(3)	0.114(5)	0.098(5)	0.090(6)	0.081(4)	0.073(5)	0.054(5)	0.052(6)		
$P^*_{L, DQD}$	0.0268(6)	0.0216(10)	0.0184(9)	0.0168(12)	0.0150(8)	0.0136(9)	0.0100(10)	0.0095(13)		
$P^*_{L, QDQ}$	0.0022(1)	0.0018(1)	0.0015(1)	0.0014(1)	0.0012(1)	0.0011(1)	0.0008(1)	0.0008(1)		
$P^*_{L, DDD4}$	-0.191(5)	-0.157(5)	-0.139(4)	-0.128(5)	-0.114(5)	-0.102(5)	-0.082(5)	-0.074(6)		
$E^*_{L, int conf.}$	-4.21(4)	-3.96(6)	-3.78(6)	-3.63(8)	-3.52(6)	-3.40(8)	-3.07(10)	-3.02(13)		
$E^*_{L, 2body}$	-4.48(4)	-4.10(7)	-3.93(7)	-3.80(9)	-3.64(7)	-3.53(8)	-3.17(11)	-3.13(14)		
$E^*_{L, DDD}$	0.209(3)	0.181(5)	0.165(5)	0.155(6)	0.145(5)	0.135(5)	0.114(5)	0.109(7)		
$E^*_{L, DDQ}$	0.054(1)	0.047(1)	0.042(1)	0.040(2)	0.037(1)	0.034(1)	0.028(2)	0.027(2)		
$E^*_{L, DQD}$	0.0087(2)	0.0075(3)	0.0067(2)	0.0063(3)	0.0058(2)	0.0054(2)	0.0044(3)	0.0043(4)		
$E^*_{L, QDQ}$	0.00062(1)	0.00053(2)	0.00047(2)	0.00044(2)	0.00041(2)	0.00038(2)	0.00031(2)	0.00030(3)		
$E^*_{L, DDD4}$	-0.067(1)	-0.059(1)	-0.055(1)	-0.052(1)	-0.048(2)	-0.044(2)	-0.039(1)	-0.036(1)		
m^*_L	-3.41	-3.28	-3.33	-3.30	-3.22	-3.20	-3.18	-3.15		
r^*_V	0.0109(17)	0.0227(27)	0.0245(27)	0.0313(36)	0.0414(45)	0.0513(67)	0.0566(46)	0.0746(33)		
$P^*_{V, int}$	0.0075(16)	0.0163(31)	0.0180(31)	0.0229(43)	0.0301(57)	0.0366(97)	0.0419(66)	0.0514(54)		
$P^*_{V, 2body}$	-0.0006(3)	-0.0025(8)	-0.0030(8)	-0.0046(11)	-0.0075(15)	-0.0113(34)	-0.0125(21)	-0.0227(20)		
$P^*_{V, DDD}$	0.0050(75)	0.0686(472)	0.0838(364)	0.148(62)	0.311(116)	0.542(177)	0.717(105)	1.546(217)		
$P^*_{V, DDQ}$	0.009(24)	0.198(151)	0.233(111)	0.411(175)	0.883(345)	1.518(472)	2.031(296)	4.365(650)		
$P^*_{V, DQD}$	0.002(50)	0.357(299)	0.400(216)	0.706(307)	1.559(640)	2.642(798)	3.573(524)	7.67(121)		
$P^*_{V, QDQ}$	-0.006(41)	0.282(251)	0.302(184)	0.534(241)	1.213(519)	2.039(613)	2.789(412)	5.969(982)		
$P^*_{V, DDD4}$	-0.0317(242)	-0.299(163)	-0.367(136)	-0.637(291)	-1.416(559)	-2.475(791)	-3.293(514)	-7.17(102)		
$E^*_{V, int conf.}$	-0.11(2)	-0.21(3)	-0.21(3)	-0.27(4)	-0.34(5)	-0.42(6)	-0.45(3)	-0.59(3)		
$E^*_{V, 2body}$	-0.11(2)	-0.21(4)	-0.21(3)	-0.27(4)	-0.35(5)	-0.42(6)	-0.45(3)	-0.60(3)		
$E^*_{V, DDD}$	0.15(25)	0.94(57)	1.08(45)	1.50(49)	2.39(66)	3.38(73)	4.12(34)	6.67(68)		
$E^*_{V, DDQ}$	0.02(7)	0.22(15)	0.25(11)	0.34(12)	0.56(17)	0.78(16)	0.95(8)	1.54(17)		
$E^*_{V, DQD}$	-0.01(13)	0.34(25)	0.36(19)	0.49(17)	0.83(27)	1.15(23)	1.42(13)	2.29(27)		
$E^*_{V, QDQ}$	-0.02(9)	0.23(18)	0.24(14)	0.32(12)	0.56(19)	0.77(16)	0.96(9)	1.55(19)		
$E^*_{V, DDD4}$	-0.078(65)	-0.307(144)	-0.356(120)	-0.479(168)	-0.815(237)	-1.158(234)	-1.415(127)	-2.316(241)		
m^*_V	-3.50	-3.34	-3.38	-3.32	-3.23	-3.19	-3.20	-3.13		

The coexistence properties obtained from argon using the BFW potential are summarised in Table 3.1 and the BFW + three-body calculations are reported in Table 3.4. In Figure 3.1, experimental data for the vapour-liquid phase envelope of argon are compared with simulation results obtained in this work and data reported by Anta et al. [Ant97] for the Aziz-Slaman [Azi86] and Aziz-Slaman + Axilrod-Teller intermolecular potentials. The comparison with experiment in Figure 3.1 indicates that both the BFW and Aziz-Slaman potentials do not predict the liquid phase coexisting density of argon adequately. There is generally fair agreement for the vapour-branch of the coexistence curve. This contrasts with calculations using the Lennard-Jones potential, which normally yields good agreement with experiment for liquid densities. The good agreement often reported [Sad96b] with the Lennard-Jones potential is fortuitous and probably arises for the “effective” many-body nature of the potential. It is apparent from Figure 3.1 that genuine two-body potentials cannot predict the liquid phase densities of argon adequately. The results obtained from the BFW and Aziz-Slaman potentials are almost identical.

Anta et al. [Ant97] reported that the addition of the Axilrod-Teller term to the Aziz-Slaman potential [Azi86, Azi93] resulted in a considerable improvement in the agreement between theory and experiment as illustrated in Figure 3.1. In Figure 3.1 we also show that the addition of the three-body term to the BFW potential results in good overall agreement of theory with experimental data. The absolute average deviations (AAD) [Sad95] for the vapour and liquid densities are 36.4% and 2.3%, respectively. The lower the value of the AAD, the closer the simulation values are with the experimental data. The experimental liquid branch of the coexisting phase curves is well reproduced by our results. The agreement with the vapour branch is not equally good. It should be noticed from the simulation data, that the three-body contribution to the total

potential energy is less than 0.7% in the vapour side (in the liquid side it is greater than 3%). This means that the inclusion of three body potentials does not significantly affect the properties of the vapour. That is why we have similar results in the vapour side for the simulations with only the two-body potential and the simulations with two-body + three-body potentials. The work of Anta et al. [Ant97, see Figure 3.1] for the Aziz + AT potentials shows that the calculated vapour branch is shifted closer towards the experimental curve. However, the AAD is about 10%. Therefore, even if their results are more accurate, it seems that the inclusion of the three-body potentials is not sufficient to reproduce the experimental data. We believe that this is due to a lack of accuracy of the two-body potential for vapour densities. Interestingly, in their work on argon, Leonhard and Deiters [Leo00] observed behaviour similar to our findings using the Hloucha ab initio potential [Dei99] + AT potential. Using their own ab initio potential + AT they found a behaviour similar to Anta et al.

The contributions to both pressure and configurational energy of the various multipole terms to the three-body interactions of argon are identified in Table 3.4. The contribution of three-body interactions to the vapour phase is negligible whereas they make an important contribution to the liquid phase. The various three-body contributions to the configurational energy of the liquid phase of argon are compared graphically in Figure 3.2. Although Anta et al. [Ant97] reported values of density, temperature, pressure and configurational energies, they did not report the contribution of three-body interactions to either the pressure or energy. It is evident from both the data in Table 3.4 and the comparison in Figure 3.2 that the triple-dipole term makes the dominant contribution to three-body interactions. The other third-order multipole interactions ($u_{DDQ} + u_{DQQ} + u_{QQQ}$) contribute approximately 32% of the triple-dipole term. However, the effect of this contribution is offset largely by an approximately

equal contribution (26% of the triple-dipole term) from fourth-order triple-dipole interactions of opposite sign. A similar behaviour is seen by the three-body contributions of the pressure. Consequently, the Axilrod-teller term alone is an excellent approximation of three-body dispersion interaction. This conclusion is consistent with earlier work [Dor71] on the relative magnitude of three-body interactions. It is also consistent with other work [Bar72b] on the relative contributions of three-body interactions to the third virial coefficient.

To the best of our knowledge, previous work on the effect of three-body interactions on the phase behaviour of fluids has been confined exclusively to argon. In Tables 3.2, 3.3, 3.5 and 3.6 we report calculations for the vapour-liquid coexistence of krypton and xenon. The coexistence properties calculated from two-body potentials are summarised in Tables 3.2 (krypton) and 3.3 (xenon) whereas calculations including two-body and three-body terms are found in Tables 3.5 (krypton) and 3.6 (xenon). The krypton and xenon atoms are considerably larger than argon and it can be anticipated that their increased polarizability may result in an increase in the relative importance of three-body interactions. The comparison of experiment with theory for the vapour-liquid coexistence of krypton and xenon is illustrated in Figures 3.3 and 3.4, respectively. For both krypton and xenon, the two-body potentials fail to represent the liquid phase densities adequately whereas there is generally fair agreement for the vapour phase. However, it is evident that the addition of three-body interactions results in very good agreement of theory with experiment for sub-critical liquid-phase densities. For krypton, the AAD for the vapour and liquid densities are 34.5% and 1.9% respectively. For xenon, the average absolute deviations for the vapour and liquid densities are 35.8% and 1.4%, respectively. It should be stressed that in all cases the agreement between theory

and experiment represent genuine predictions and no attempt has been made to optimise the agreement by altering the intermolecular potential parameters.

The relative contribution of the various multipole terms (Tables 3.5 and 3.6) to the three-body interactions of krypton and xenon is similar to that observed for argon. Interestingly, for xenon, the magnitude of the contribution from the fourth order triple-dipole term ($DDD4$) is actually slightly greater than the dipole-dipole-quadrupole (DDQ), dipole-quadrupole-quadrupole (DQQ) and triple-quadrupole (QQQ) terms combined. Therefore, for krypton and xenon, the Axilrod-Teller term alone is a good representation of three-body interactions because the contribution of other multipole terms is offset by the contribution from the fourth-order triple dipole term.

In Figure 3.5 we report the logarithm of the total pressure (two-body + three-body) versus the inverse of the temperature, for argon, krypton and xenon. The experimental data [Var75] are also shown. We plot only the vapour pressure because the liquid pressure is characterized by large errors. The simulated pressure is shifted down in comparison with the experimental data. This is simply due to the density shift observed in the vapour branch. In fact, for the vapour the main contribution to pressure comes from the ideal part, $P \approx T \times \mathbf{r}$ (see Eq. (2.65)), so an inaccuracy in the density causes an inaccuracy in the pressure.

A significant error relative to the total pressure in the liquid side occurs because the kinetic part and potential part of the pressure are very similar but with opposite sign. For example if we consider in Table 3.4 the value of the temperature $T^* = 0.9$ and the relative liquid density $\mathbf{r}^* = 0.639$, the kinetic pressure is $P_{kin}^* = T^* \times \mathbf{r}^* \approx 0.575$. The potential part is:

$$P_{Lpot}^* = P_{L2body}^* + P_{LDDD}^* + P_{LDDQ}^* + P_{LDQ}^* + P_{LQQ}^* + P_{LDDD4}^* \approx -0.54.$$

The total pressure is $P_{tot}^* \approx 0.035$ which is just 15% of the two different contributions. Thus a small fluctuation in the values of both kinetic and potential parts can cause a significant fluctuation in the total pressure.

This work has not considered the possibility of interactions from three-body repulsion. Sadus and Prausnitz [Sad96b] used a three-body repulsive potential [She66] in conjunction with Lennard-Jones and AT potentials. They found that three-body repulsion may offset the contribution of Axilrod-Teller interactions by as much as 45%. However, this conclusion is based largely on approximate models [She66] of three-body repulsion that are tied closely to the Lennard-Jones potential. It has been suggested [Rit90] that three-body repulsion may improve the prediction of the thermodynamic properties of xenon. Recently, Bukowsky and Szalewicz [Buk01] reported calculations for argon using an *ab initio* potential, which includes three-body repulsion potentials [Lot97b]. They found that the triple-dipole potential alone is an excellent approximation of the total three-body energy because the other contributions cancel. Also our good results obtained for argon, krypton and xenon without including three-body short-range terms may indicate that those potentials do not contribute significantly to the vapour-liquid coexistence. Bukowsky and Szalewicz attribute the cause of the small discrepancies to the neglected quantum effects. Barker et al. [Bar71a] showed that these quantum effects are repulsive and amount to 15-17% of the three-body contributions. They inferred that their inclusion might bring the calculated coexistence curve even closer to the experimental data.

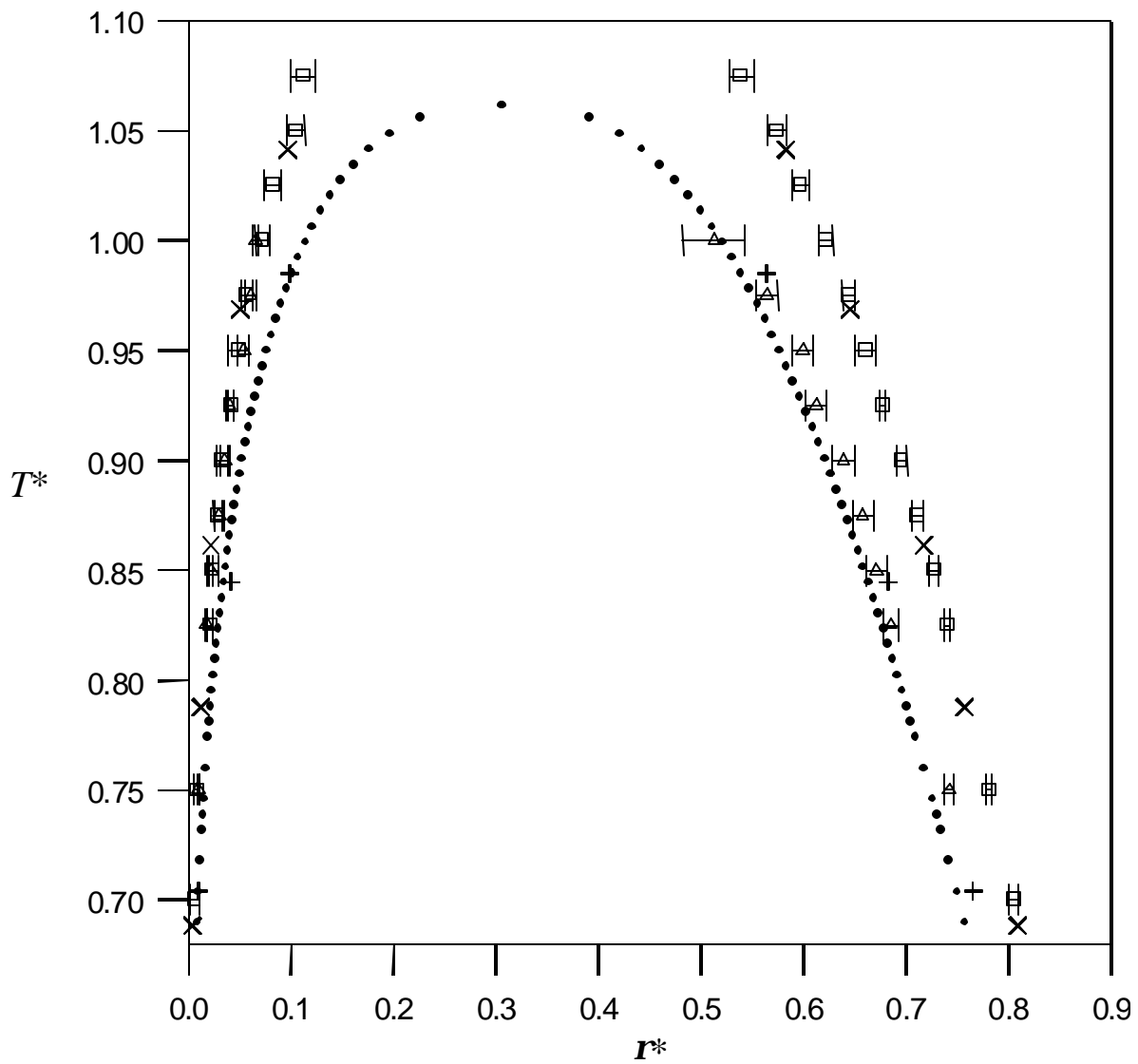


Figure 3.1 Comparison of experiment (\bullet , [Var75]) with calculation using the BFW potential [Bar71a] (\square), the Aziz-Slaman potential (\times , [Ant97]), the Aziz-Slaman + Axilrod-Teller ($+$, [Ant97]) and the BFW + three-body ($DDD + DDQ + DQQ + QQQ + DDD4$) potentials ($+$) for the vapour-liquid coexistence of argon.

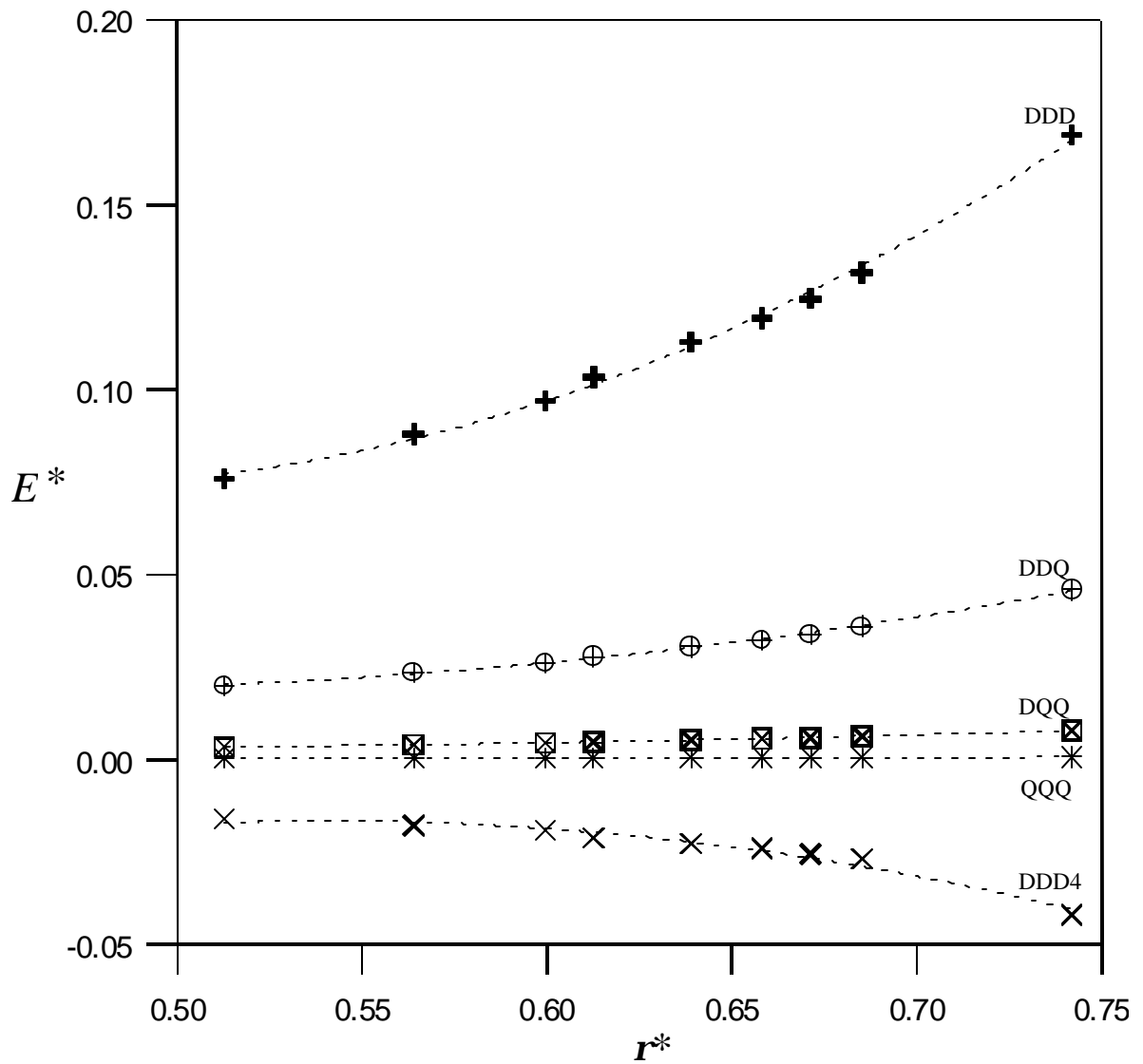


Figure 3.2. Comparison of the contribution of the various three-body terms to the configurational energy of the liquid phase of argon.

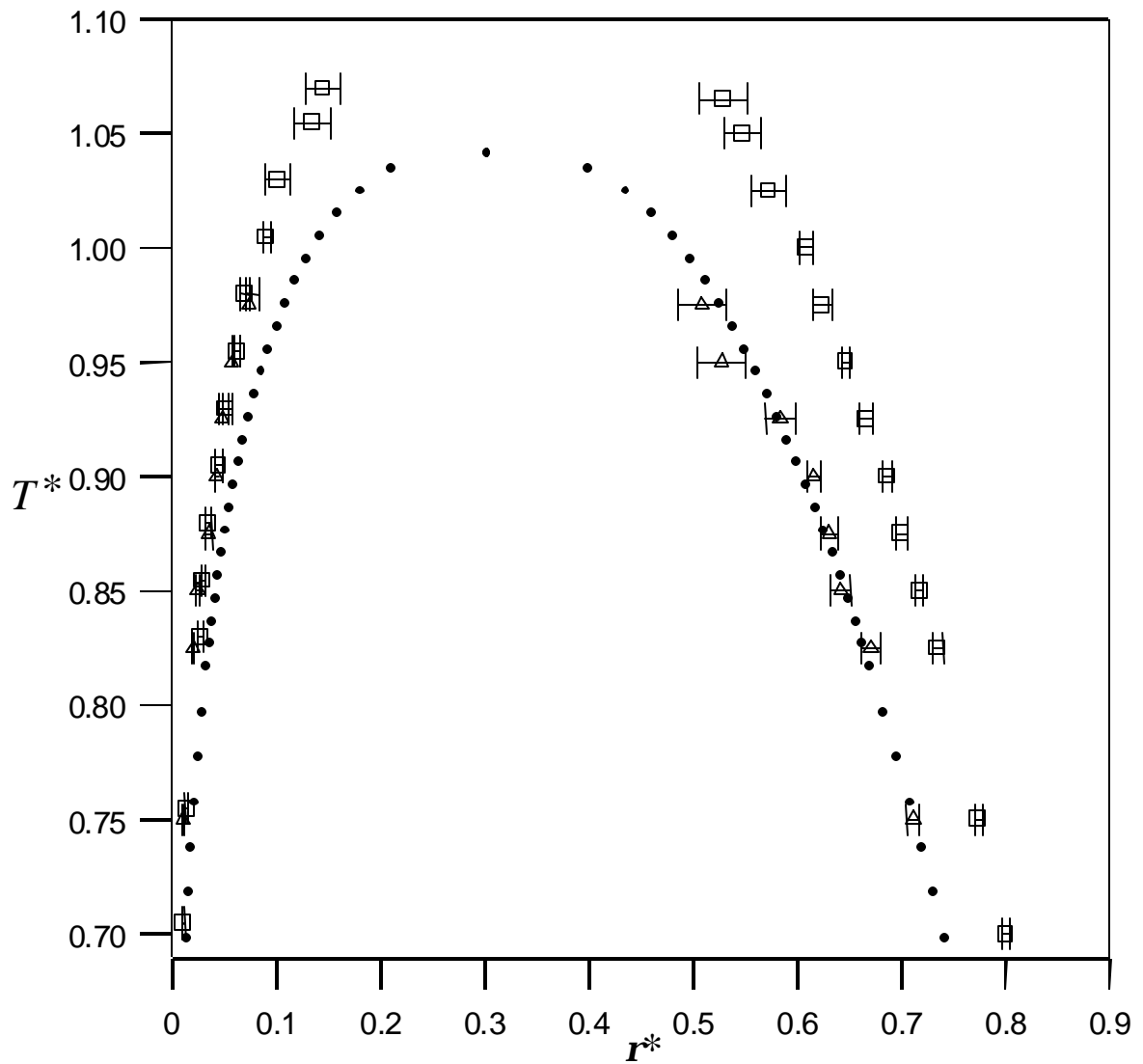


Figure 3.3 Comparison of experiment (\bullet , [Var75]) with calculation using the two-body potential of Barker et al. [Bar74] (\square) and the Barker et al. [Bar74] + three-body ($DDD + DDQ + DQQ + QQQ + DDD4$) potentials ($+$) for the vapour-liquid coexistence of krypton.

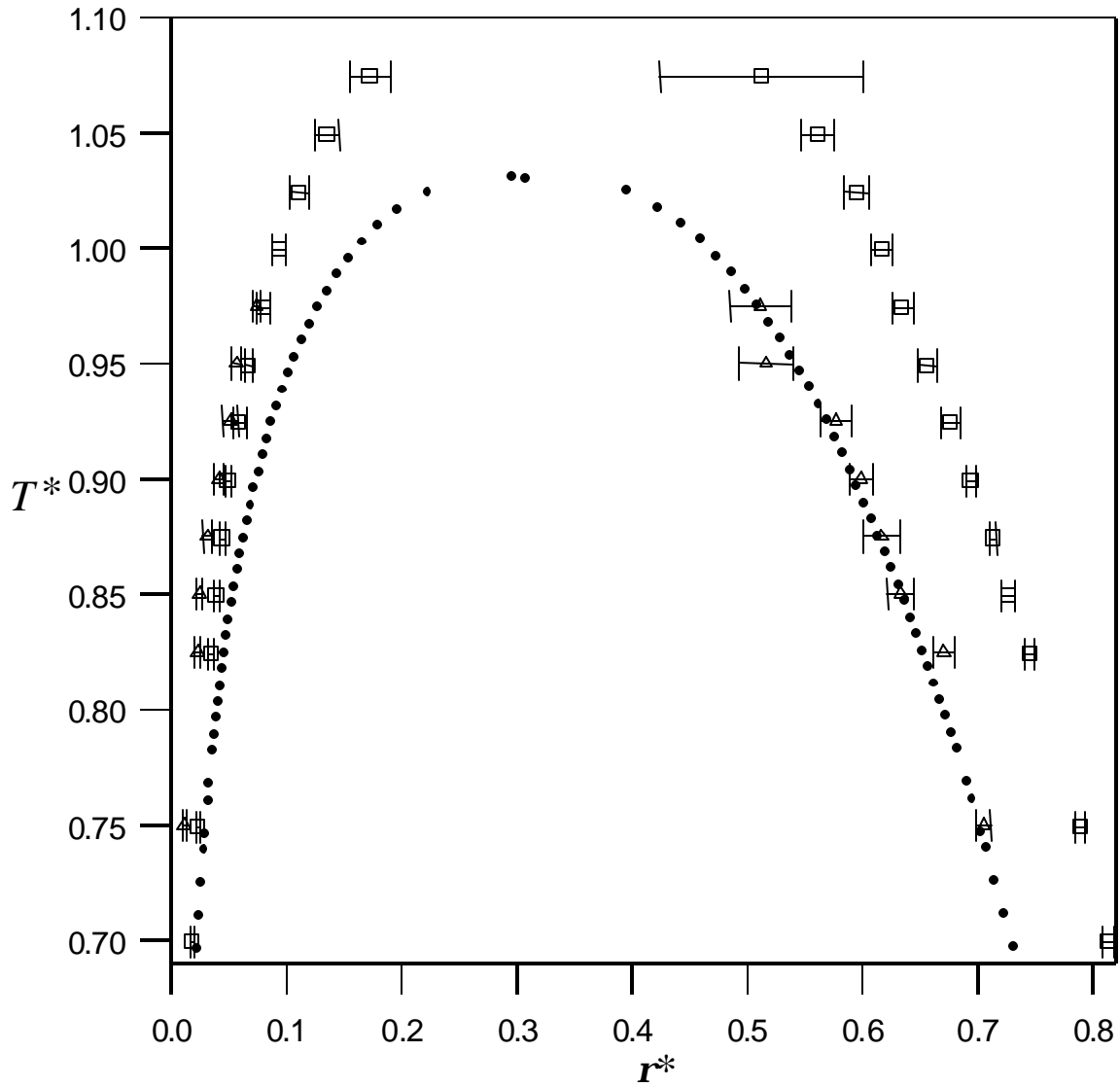


Figure 3.4 Comparison of experiment (\bullet , [Var75]) with calculation using the two-body potential of Barker et al. [Bar74] (\square) and the Barker et al. [Bar74] + three-body ($DDD + DDQ + DQQ + QQQ + DDD4$) potentials ($+$) for the vapour-liquid coexistence of xenon.

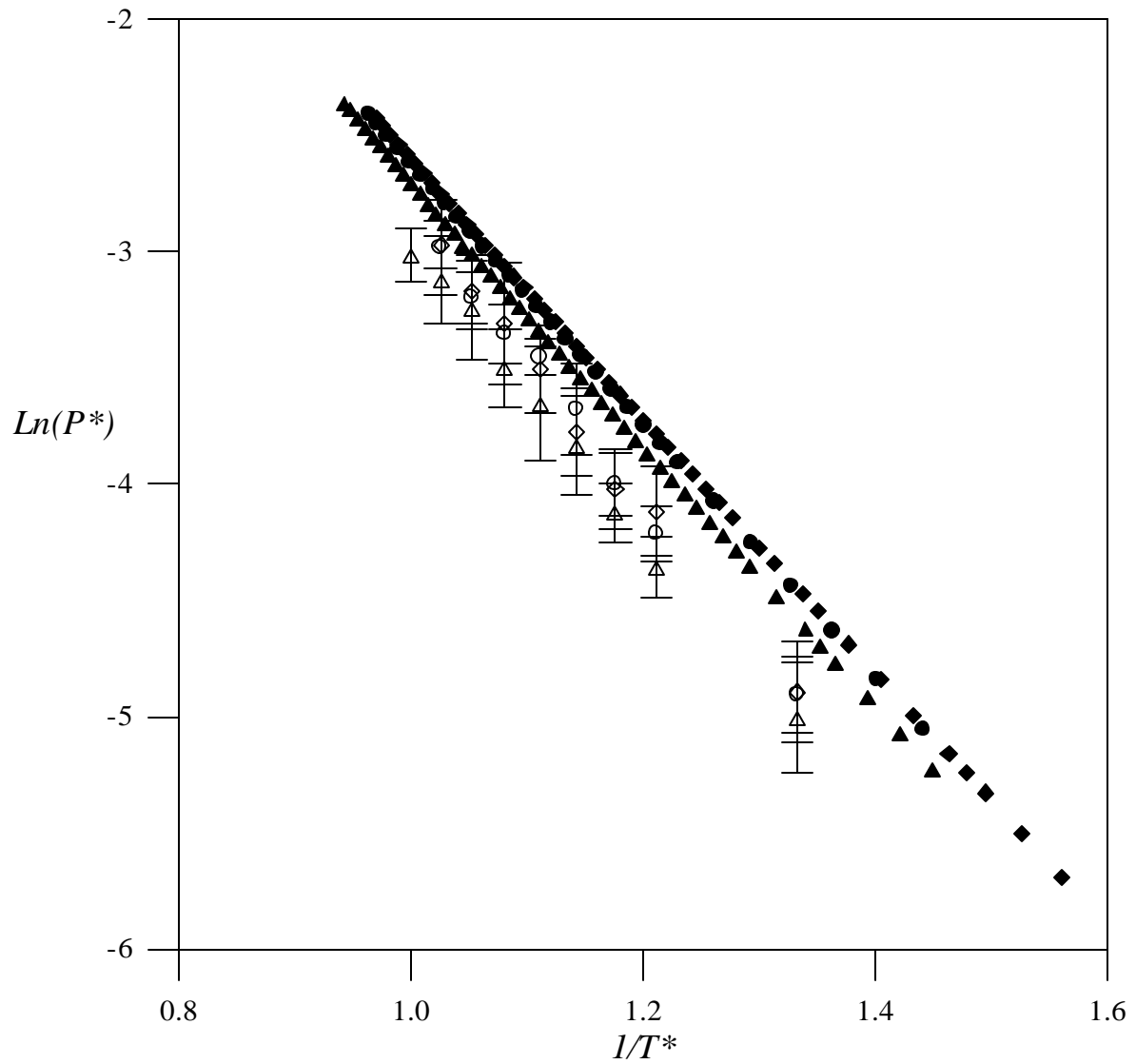


Figure 3.5 Logarithm of the pressure vs. the inverse of the temperature. Comparison between simulation results (Argon +, krypton O, xenon ◇) and experimental data [Var75] (Argon ▲, krypton ●, xenon ◆)

Argon-krypton mixture

The results of Gibbs ensemble simulations for the vapour-liquid properties of argon + krypton are reported in Tables 3.7 and 3.8. In Tables 3.7 and 3.8, x denotes the mole fraction of the liquid (L) and vapour (V) phases. The motivation for studying the argon + krypton mixture is that it provides a rare example of a binary mixture for which quantitatively accurate intermolecular potentials are available. Therefore, comparison of the results of two-body only simulations with two-body + three-body simulations allows us to make observations concerning the role of three-body interactions. Calculations were performed for both two-body and two-body + three-body terms. The temperature of $T^* = 1.148$ (163.15 K) was selected because the vapour-liquid envelope at this temperature is representative of the vapour-liquid phase of the argon + krypton system. Since for pure fluids we found that the two-body + AT potentials represent the dominant terms, we did not include the other multipole three-body terms (see Chapter 2).

A comparison of theory with experiment for the pressure-composition behaviour of argon + krypton is illustrated in Figure 3.6. In general, there is good agreement between theory and experiment [Sch75] for the overall phase envelope. The liquid-phase properties are predicted accurately whereas there are noticeable deviations from experiment for the vapour-phase branch of the coexistence curve. These observations are consistent with the calculations reported for pure component phase equilibria in section 3.1. Interestingly, the results for two-body only and two-body + three-body calculations are almost identical. At a given pressure, three-body interactions do not appear to have a significant role in determining the coexistence composition. This is despite the fact that the data in Table 3.8 indicates that three-body interactions typically contribute approximately 5% of the overall configurational energy.

The pressure-density behaviour of the argon + krypton mixture is illustrated in Figure 3.7. The coexistence density of the vapour-branch is unaffected by three-body interactions. In contrast, Figure 3.7 indicates that three-body interactions can significantly affect the coexisting liquid-phase density. Experimental density data is not available for comparison with the calculations. In section 3.1 we have reported a similar density-shift for the vapour-liquid equilibria of pure noble gases resulting in good agreement with experimental data. The reduction in the liquid-phase density can be attributed to an increase in volume caused by an additional repulsive influence of the three-body term.

Table 3.7 Molecular simulation results for the vapour-liquid equilibria of argon + krypton at $T^* = 1.148$ using the two-body potential.

P^*	x_L^{Kr}	x_V^{Kr}	P_{Ltot}^*	P_{Vtot}^*	r_L^*	r_V^*	E_{L2b}^*	E_{V2b}^*	m_{LKr}^*	m_{VKr}^*	m_{LAr}^*	m_{VAr}^*
0.0350	0.831(5)	0.544(25)	0.019(40)	0.031(6)	0.618(6)	0.032(3)	-6.00(6)	-0.39(4)	-5.12	-5.08	-5.10	-5.12
0.0445	0.760(11)	0.409(18)	0.066(44)	0.039(7)	0.619(6)	0.042(4)	-5.80(9)	-0.41(5)	-5.04	-5.23	-4.66	-4.62
0.0495	0.680(9)	0.329(38)	0.067(43)	0.048(17)	0.613(8)	0.055(9)	-5.50(8)	-0.51(10)	-5.34	-5.33	-4.48	-4.25
0.0543	0.665(8)	0.323(24)	0.062(40)	0.052(11)	0.620(8)	0.060(7)	-5.52(10)	-0.57(7)	-5.25	-5.28	-4.25	-4.18
0.0642	0.547(7)	0.257(30)	0.064(49)	0.058(15)	0.600(8)	0.067(8)	-5.01(7)	-0.63(12)	-5.62	-5.51	-4.02	-3.99
0.0737	0.475(6)	0.216(18)	0.091(47)	0.067(19)	0.605(9)	0.093(10)	-4.85(9)	-0.82(9)	-5.48	-5.60	-3.88	-3.75
0.0787	0.432(5)	0.177(18)	0.092(55)	0.070(20)	0.596(14)	0.095(10)	-4.66(12)	-0.80(10)	-5.73	-5.80	-3.69	-3.66
0.0837	0.385(4)	0.175(14)	0.106(52)	0.074(39)	0.592(10)	0.103(19)	-4.51(8)	-0.86(17)	-5.73	-5.80	-3.66	-3.63
0.0933	0.319(5)	0.148(12)	0.069(48)	0.082(29)	0.577(6)	0.121(13)	-4.23(3)	-1.00(13)	-5.96	-5.99	-3.58	-3.52
0.0986	0.266(5)	0.138(13)	0.070(55)	0.088(40)	0.573(14)	0.168(16)	-4.08(11)	-1.36(15)	-6.20	-6.14	-3.44	-3.40
0.1041	0.225(6)	0.115(11)	0.113(30)	0.097(36)	0.573(8)	0.165(16)	-3.98(6)	-1.31(14)	-6.36	-6.30	-3.40	-3.36

Table 3.8 Molecular simulation results for the vapour-liquid equilibria of argon + krypton at $T^* = 1.148$ using the two-body + three-body intermolecular potential.

	P^*										
	0.035	0.0445	0.0495	0.0543	0.0642	0.0737	0.0787	0.0837	0.0933	0.0986	0.1041
$\chi_L(Kr)$	0.847(5)	0.738(5)	0.688(15)	0.624(3)	0.556(11)	0.474(6)	0.445(9)	0.389(5)	0.312(4)	0.264(2)	0.221(6)
$\chi_V(Kr)$	0.579(20)	0.429(19)	0.380(23)	0.332(14)	0.292(25)	0.234(19)	0.208(10)	0.184(16)	0.154(9)	0.133(6)	0.119(12)
$P_{L,hor}^*$	0.029(85)	0.039(55)	0.048(72)	0.071(62)	0.083(75)	0.086(79)	0.059(81)	0.073(76)	0.069(50)	0.081(86)	0.096(78)
$P_{V,hor}^*$	0.033(7)	0.036(7)	0.044(11)	0.047(18)	0.063(24)	0.066(19)	0.063(19)	0.069(19)	0.079(22)	0.080(14)	0.090(19)
P_{L2b}^*	-0.973(47)	-0.918(44)	-0.886(51)	-0.828(30)	-0.812(50)	-0.764(54)	-0.737(40)	-0.713(34)	-0.661(21)	-0.563(45)	-0.574(40)
P_{V2b}^*	-0.0086(22)	-0.0085(26)	-0.0131(37)	-0.0144(68)	-0.0267(80)	-0.0353(82)	-0.0245(71)	-0.0367(74)	-0.0446(91)	-0.0479(58)	-0.0668(66)
P_{L3b}^*	0.340(22)	0.304(7)	0.282(11)	0.261(17)	0.246(12)	0.214(11)	0.186(17)	0.177(18)	0.145(12)	0.111(13)	0.115(13)
P_{V3b}^*	0.00024(11)	0.00020(8)	0.00040(15)	0.00039(29)	0.00126(59)	0.00147(49)	0.00108(43)	0.00164(48)	0.00261(83)	0.00279(42)	0.00428(97)
r_L^*	0.577(13)	0.569(4)	0.568(9)	0.556(13)	0.566(11)	0.554(12)	0.532(20)	0.530(21)	0.510(15)	0.464(24)	0.483(23)
r_V^*	0.036(4)	0.038(4)	0.049(6)	0.053(10)	0.077(13)	0.087(9)	0.075(10)	0.090(9)	0.105(11)	0.109(7)	0.133(10)
E_{L2b}^*	-5.65(14)	-5.27(4)	-5.12(11)	-4.85(11)	-4.74(11)	-4.44(11)	-4.21(17)	-4.07(15)	-3.76(11)	-3.37(15)	-3.39(15)
E_{V2b}^*	-0.44(8)	-0.40(4)	-0.49(7)	-0.49(13)	-0.71(13)	-0.75(9)	-0.65(8)	-0.76(7)	-0.88(10)	-0.89(5)	-1.04(8)
E_{L3b}^*	0.196(8)	0.178(3)	0.165(4)	0.156(7)	0.144(5)	0.129(4)	0.116(7)	0.111(7)	0.094(5)	0.079(5)	0.079(5)
E_{V3b}^*	0.0021(8)	0.0017(4)	0.0026(8)	0.0021(11)	0.0051(17)	0.0054(14)	0.0046(11)	0.0058(11)	0.0080(19)	0.0083(9)	0.0105(17)
$\Pi_L(Kr)$	-4.9	-5.16	-5.02	-5.31	-5.37	-5.49	-5.62	-5.7	-5.9	-5.98	-6.24
$\Pi_V(Kr)$	-4.96	-5.23	-5.21	-5.32	-5.32	-5.49	-5.66	-5.76	-5.9	-6.06	-6.19
$\Pi_L(Ar)$	-5.11	-4.63	-4.33	-4.23	-3.9	-3.75	-3.82	-3.67	-3.57	-3.52	-3.41
$\Pi_V(Ar)$	-5.15	-4.72	-4.44	-4.29	-3.98	-3.79	-3.83	-3.68	-3.57	-3.51	-3.41

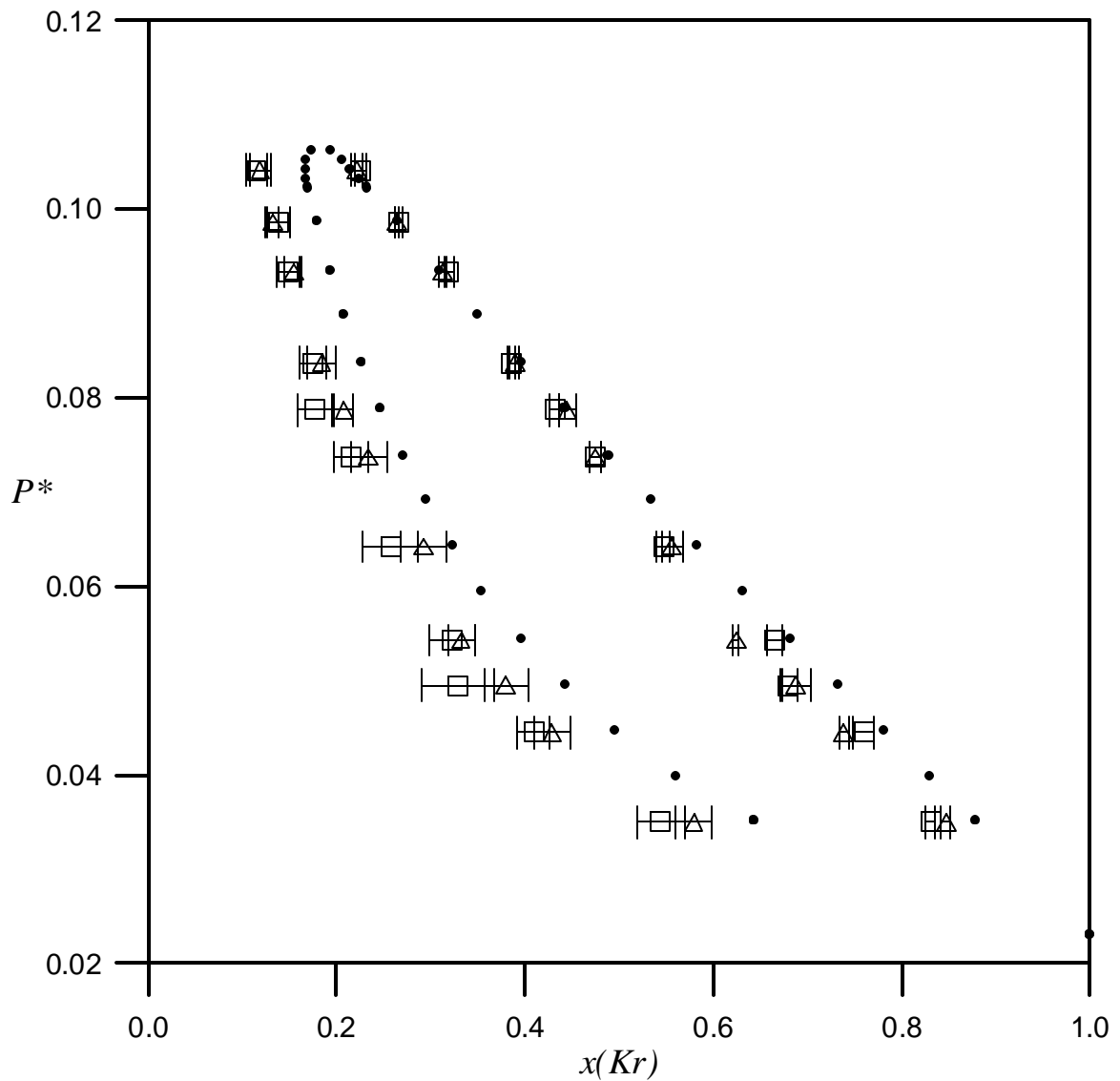


Figure 3.6 Comparison of experimental vapour-liquid equilibria at $T^* = 1.148$ (163.15 K) (●, [Sch75]) with calculations using only two-body (□) and two-body + three-body (△) intermolecular potentials of argon + krypton.

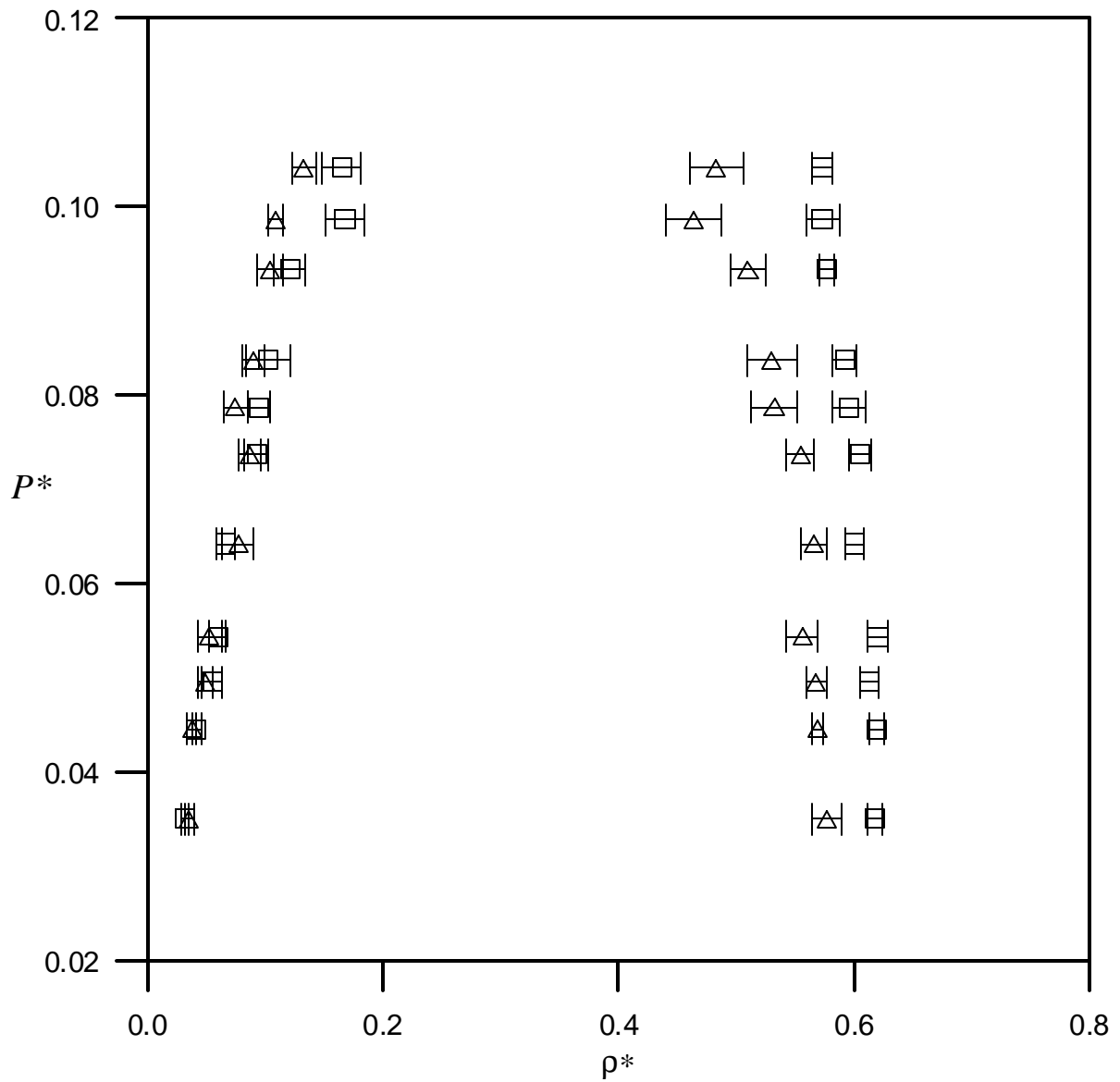


Figure 3.7 Comparison of the effect of two-body only (\square) and two-body + three-body (Δ) interactions on the vapour and liquid coexistence densities and pressures of argon + krypton.

3.2 A simple relationship between two-body and three-body potentials

The introduction of the three-body potential increases the computing time of a normal two-body potential simulation by a factor of ten. This is the main reason to adopt an effective potential that accounts for the three-body effects without incurring expensive routine calculations. Several effective potentials have been proposed [Cop68, Mur71, Miy94, Ste94, van99]. Smit et al. [Smi92] pointed out that a convenient way to account for three- and higher-body interactions consists in using pair potentials that depend on the density. In their work they report the equation of state of a fluid with a particular class of density-dependent potential in terms of the equation of state and energy of a reference fluid.

Analyzing the data from *NVT* Gibbs ensemble simulations shown in previous sections, we noticed that two- and three-body potential energies are linked by a simple relationship. We also performed standard *NVT* Monte Carlo [Sad99] simulations for 500 atoms of argon, krypton and xenon, to check if this relationship holds for different systems. The simulations were performed in cubic boxes, and the conventional periodic boundary conditions were applied [Sad99]. For pair interactions, long-range corrections were used to recover the full contribution to the intermolecular potential (see Appendix 1), whereas three-body interactions were assumed to be zero at separations greater than a quarter of the box length (see Appendix 2). A total of 40000 cycles were used with averages being accumulated after 20000 cycles. The two-body energy (E_2) was obtained by averaging the contribution of the pair potential over all distinct pairs of atoms, whereas the three-body energy (E_3) is the average of the Axilrod-Teller potential for all distinct triplets of atoms.

The ratio of three-body (E_3) to two-body (E_2) energies obtained from *NVT* Gibbs ensemble simulations is shown in Figure 3.8 as a function of reduced number density, \mathbf{r}^* . Also results from *NVT* Monte Carlo simulations, reported in Table 3.9, are shown in Figure 3.8 to supplement Gibbs ensemble data. The temperatures used covered the temperature range for vapour-liquid coexistence of a pure fluid.

Table 3.9 *NVT* Monte Carlo simulation results for argon, krypton and xenon at different densities and temperatures.

	\mathbf{r}^*	T^*	E_{AT}^*	E_{2b}^*	P_{AT}^*	P_{2b}^*
<i>Ar</i>	0.350	1.30	0.031(1)	-1.97(2)	0.033(1)	-0.24(5)
	0.400	1.20	0.044(2)	-2.35(2)	0.053(2)	-0.33(7)
<i>Kr</i>	0.450	1.25	0.068(2)	-2.63(4)	0.091(2)	-0.36(9)
	0.475	1.00	0.074(1)	-2.82(1)	0.106(2)	-0.59(5)
<i>Xe</i>	0.375	1.20	0.058(2)	-2.17(2)	0.065(2)	-0.29(5)
	0.425	1.00	0.075(2)	-2.54(2)	0.095(3)	-0.49(4)

It is apparent that the ratio is a linear function of density which is consistent with theoretical considerations [Ste94, Mur71]. Furthermore, within the statistical uncertainties of the simulation, the results for argon, krypton and xenon appear to obey the same relationship. A least-squares fit of the simulation data for argon, krypton and xenon yields the following empirical relationship between two-body and three-body energies:

$$E_3 = -\frac{2nrE_2}{3e\mathbf{s}^6} \quad (3.3)$$

As E_2 is generally negative, E_3 is positive which is consistent with simulation data. The above equation is a remarkably simple result that fits all the simulation data with an average absolute deviation of 2.0 %. The only constants in Eq. (3.3) are the triple-dipole

coefficient n , and the pair potential parameters e and s . The relationship is independent of temperature for the range of densities at which the fluid is normally a liquid.

The benefit of Eq. (3.3) is that an accurate estimate of the three-body energy contribution for fluid densities can be obtained from two-body calculations alone. To test the accuracy of this relationship, we performed Gibbs ensemble simulations for the phase equilibria of argon with the energies calculated from the BFW potential plus the contribution from Eq. (3.3). The Gibbs ensemble calculations were performed by first determining the contribution of two-body interactions. The two-body contribution was used in Eq. (3.3) to determine the contribution of three-body interactions. The combined two-body and three-body energies were then used to determine the acceptance of the Monte Carlo move. The results of these calculations are compared in Figure 3.9 with both experimental data [Var75] and the full two-body + three-body calculation reported in section 3.1 [Mar99]. The comparison indicates that the results obtained using Eq. (3.3) are nearly identical to the full two-body + three-body calculations.

It should be noted that, strictly speaking, the validity of the relationship is tied to the pair and three-body potentials used in the simulations, and only three different atomic species were considered. However, if these potentials genuinely reflect the contribution of two-body and three-body interactions, the result could be valid generally. We emphasise that the relationship should not be used for effective potentials such as the Lennard-Jones potential. The accuracy of the single relationship for argon, krypton and xenon may also indicate that the result is valid for other atoms.

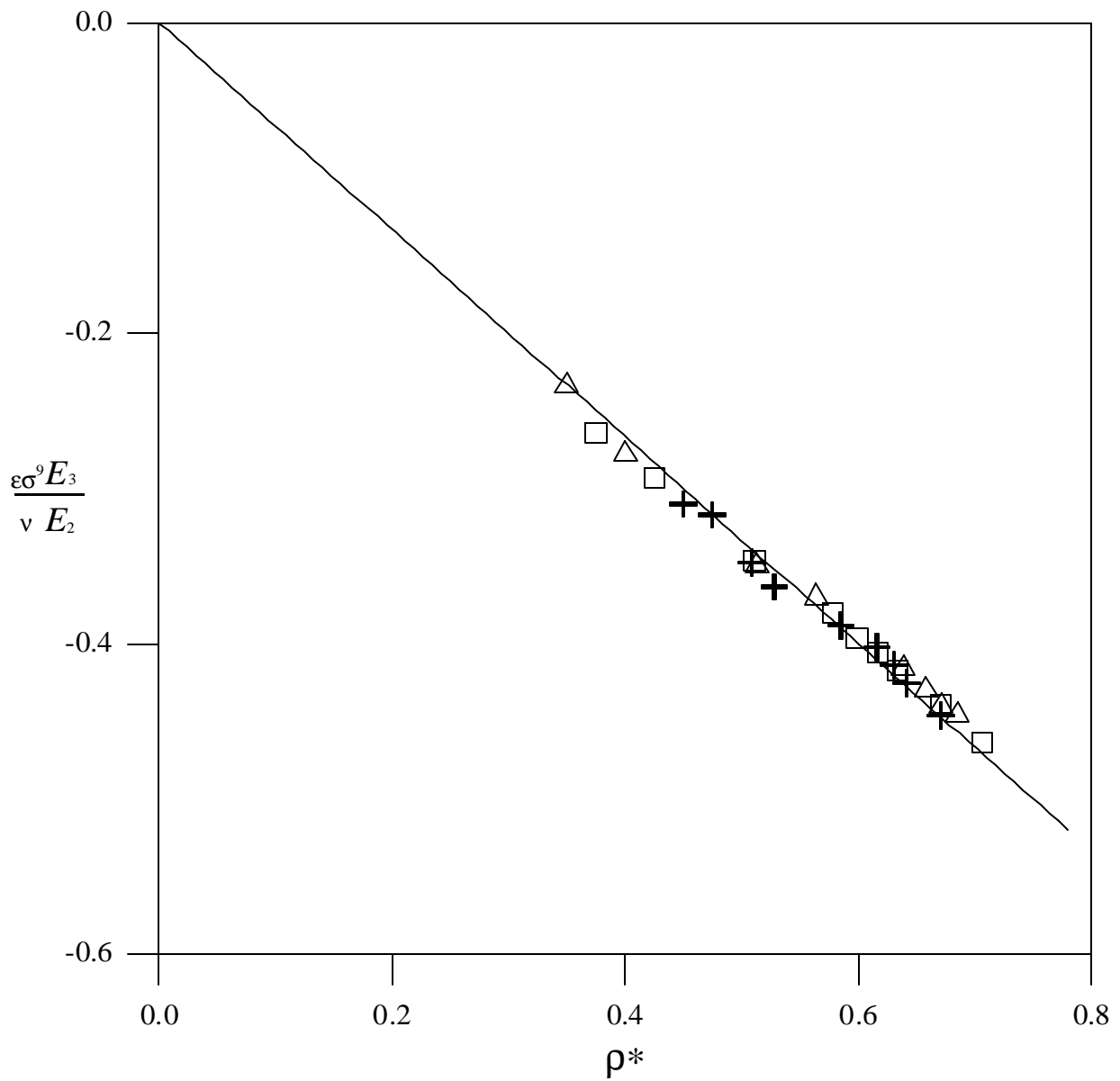


Figure 3.8 The ratio of three-body and two-body energies obtained from molecular simulation at different reduced densities. Results are shown for argon (Δ), krypton (+) and xenon (\square). The line through the points was obtained from Eq. (3.3).

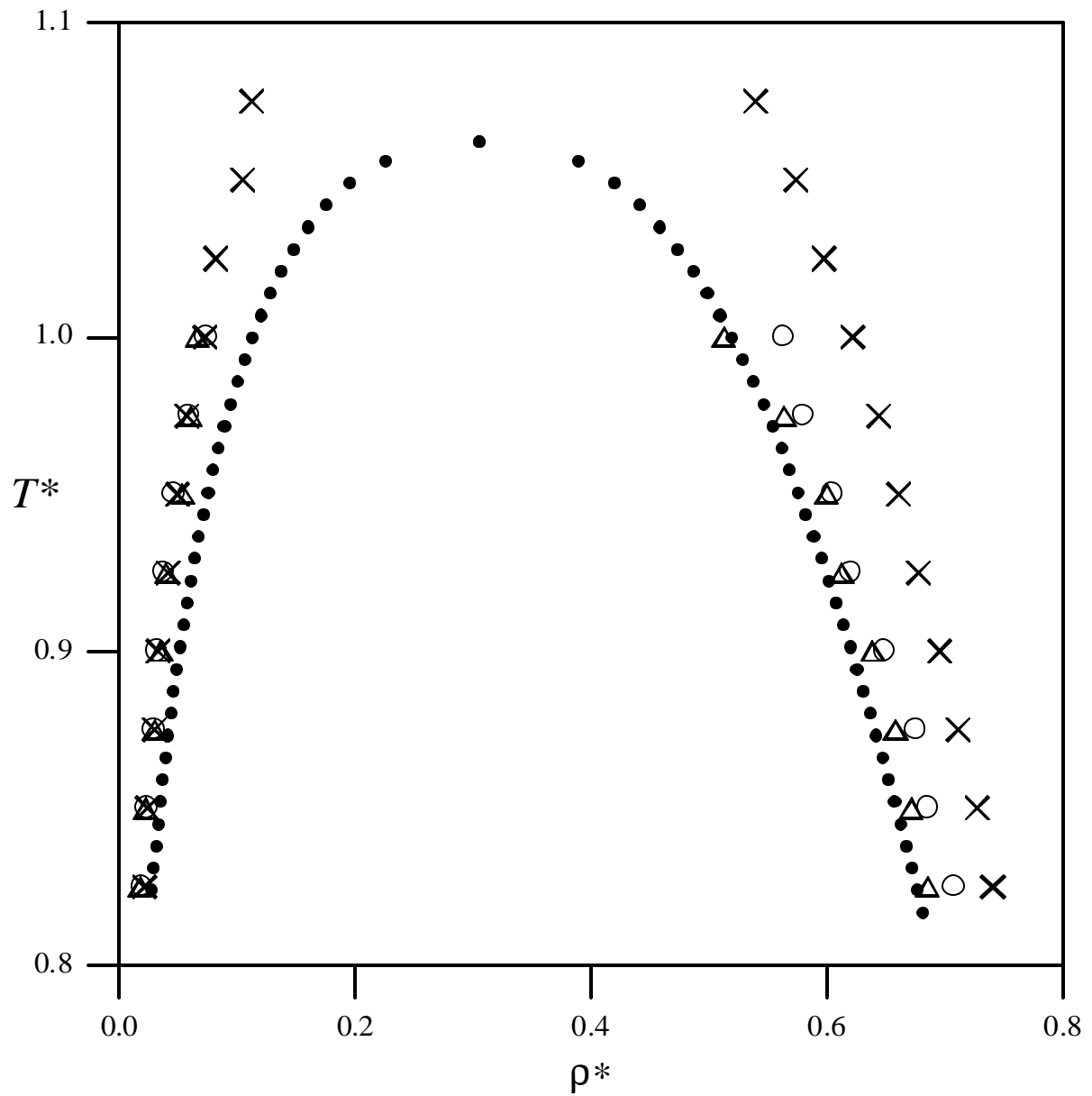


Figure 3.9 Comparison of NVT Gibbs ensemble calculations with experiment (●) [Var75] for the vapour-liquid equilibria of argon in the reduced temperature-density projection. Results are shown for the BFW potential (×), the BFW + Axilrod-Teller potential (Δ) and the BFW + three-body contribution from Eq. (3.3) potential (○).